Supplementary Information: Early Mars valley networks require decoupled surface water and groundwater

Eric Hiatt[1,2,3,4*], Mohammad Afzal Shadab[5,6], Sean P. S. Gulick[1,2,3], Timothy A. Goudge[2,3], Marc A. Hesse[2,3,7]

[1*]University of Texas Institute for Geophysics, The Jackson School of Geosciences, The University of Texas at Austin, 10601 Exploration Way Building 196, Austin, 78758, TX, U.S.A..
[2]The Department of Earth and Planetary Sciences, The Jackson School of Geosciences, The University of Texas at Austin, 2305 Speedway, Austin, 78712, TX, U.S.A..
[3]The Center for Planetary System Habitability, The University of Texas at Austin, 2305 Speedway, Austin, 78712, TX, U.S.A..
[4]Department of Earth, Environmental, and Planetary Sciences, Washington University in St. Louis, One Brookings Drive, St. Louis, 63130, MO, U.S.A..
[5]Department of Civil and Environmental Engineering, Princeton University, 54 Olden Street, Princeton, 08544, NJ, U.S.A..
[6]Integrated Ground Water Modeling Center, High Meadows Environmental Institute, Princeton University, 11 Ivy Lane, Princeton, 08544, NJ, U.S.A..
[7]Oden Institute for Computational Engineering and Sciences, The University of Texas at Austin, 01 E 24th St, Austin, 78712, TX, U.S.A..

*Corresponding author(s). E-mail(s): eric.hiatt@utexas.edu;
Contributing authors: mashadab@princeton.edu; sean@ig.utexas.edu; tgoudge@jsg.utexas.edu; mhesse@jsg.utexas.edu;

S1 Martian unconfined aquifer model

We assume a transient, unconfined aquifer in the southern highland with a vertical heterogeneity in porosity (storage) and hydraulic conductivity of the megaregolith. We use the Dupuit-Boussinesq approximation [1–3] for the elevation h of the groundwater table above the impermeable base (bedrock) of the aquifer. The dimensional governing partial differential equation for the evolution of groundwater table elevation in spherical shell coordinates [4] is The governing equation for groundwater head, h, is given by

$$\frac{\phi_0}{m+1}\frac{\partial h^{m+1}}{\partial t} - K_0 \nabla \cdot \left[\frac{h^{n+1}}{n+1}\nabla h\right] = r\,\chi(\theta,\theta_r)\Gamma(t). \tag{1}$$

where K_0 is the hydraulic conductivity coefficient, r is the nominal recharge rate prescribed at the equator, and $\chi(\theta,\theta_r)$ is a function defining the latitudinal extent and weighting of the recharge rate, where θ is the latitude and θ_r is equatorial band of precipitation that is chosen to be 45°. We assume a vertically heterogeneous hydraulic conductivity using the equation $K = K_0 z^n$ and porosity $\phi = \phi_0 z^m$, with z being the elevation from the bedrock and m and n being the power law coefficients. Compared with the data from the continental crust, their value is $m = 2.54$ and $n = 7.62$, as derived in [5, 6]. The function $\Gamma(t)$, cycles through the user prescribed intervals of time where the aquifer experiences recharge ($\Gamma(t) = 1$) as well as intra-recharge intervals ($\Gamma(t) = 0$). Since the recharge depends on the spatial location (θ, ϕ), it is incorporated by the function $\chi(\theta,\theta_r)$ defined as

$$\chi(\theta,\theta_r) = \begin{cases} \cos\left(\frac{\pi|\theta|}{2\theta_r}\right) & \text{for } |\theta| < \theta_r \\ 0 & \text{otherwise} \end{cases}. \tag{2}$$

We only consider the transient state, thereby leading to a non-linear parabolic partial differential equation. The corresponding volumetric flux of groundwater is given by Darcy's law

$$\mathbf{q} = -K\nabla h. \tag{3}$$

In general, the domain, Ω, can be complicated and not simply connected due the presence of impact basins on domain $\Omega \equiv \theta \in (0,\, \theta_o(\varphi,t)) \times \varphi \in (0, 2\pi)$, where $\theta_o(\varphi)$ is a shoreline that can move with φ. We note that, in general, θ_o is not a single valued function of φ and time t.

Along the moving shoreline, the head is equal to the elevation of the shoreline above the base of the aquifer, $h(\theta_\mathrm{o}) = h_o = z_o - z_\mathrm{B}$. In circumferential direction the boundary conditions are at $\varphi = 0 = 2\pi$. So that we have the following boundary conditions

$$h(\theta_o(s,t), \varphi_o(s,t)) = h_o, \quad h(\theta,0) = h(\theta,2\pi), \quad \left.\frac{\partial h}{\partial \varphi}\right|_{\theta,0} = \left.\frac{\partial h}{\partial \varphi}\right|_{\theta,2\pi}. \tag{4}$$

for Equation (1). The South Pole is strictly part of the interior of the domain and, as such, does not need a boundary condition.

In two dimensional solutions the entire southern boundary of the domain maps to a single point so that a boundary condition cannot and should not be enforced.

S2 Numerical model

S2.1 Spatial discretization

The numerical solver utilizes a conservative, second-order central difference scheme in space and first order implicit Euler in time [7]. It employs a staggered grid configuration where hydraulic head values, h, reside at cell centers and the specific discharge, $\mathbf{q}$, is evaluated at the cell faces. Here, we consider vertically heterogeneous aquifer properties. It leads to a variable groundwater storage due to variable pore space and hydraulic conductivity based on the location of the groundwater table. Therefore, the interpolation of the hydraulic conductivity from cell centers to cell faces boils down to analytical vertical averaging and then horizontal (harmonic) numerical averaging. Because hydraulic conductivity varies with depth, the transmissivity of the saturated column depends on the instantaneous water table elevation and is therefore time variable. This vertical integration is performed analytically: the flux term $K_0\, h^{n+1}/(n+1)\,\nabla h$ in the governing equation is the exact vertical integral of $K(z)$ from the aquifer base to the water table at head h, so the time dependence of the effective conductivity is built into the nonlinearity and no separate averaging step is required. The constant $\bar{K} = K_0/(n+1)$ quoted in the main text is the full-column average over the entire aquifer thickness, used only to nondimensionalize $\bar{r}/\bar{K}$; it does not enter the flow solution itself.

This tensor-product grid discretization is facilitated by directly calculating the discrete divergence, $\mathbf{D}$, and discrete gradient, $\mathbf{G}$, operators similar to other mimetic finite difference methods [8, 9]. When discretized in Cartesian coordinates, the derivation of the direct operators can be found in [10, 11]. The one dimensional divergence and gradient operators can be used to derive the two dimensional operators using a Kronecker product. The logically rectangular gridis diffeomorphically mapped onto spherical shell coordinates using curvilinear coordinate transformation. Specifically, this is achieved using discretized facial and volumetric Jacobians.

S2.2 Discrete operators in spherical shell $(\boldsymbol{\theta}, \boldsymbol{\varphi})$ coordinates

In Cartesian coordinates, distances from cell centers and faces remain constant. However, when using our discrete operators on a planetary scale, we must employ a spherical shell geometry. The associated variables include the radial coordinate r,the co-latitude, θ, and the circumferential coordinate, φ. The basis vectors $\mathbf{e}_\mathrm{r}$, $\mathbf{e}_\theta$, and $\mathbf{e}_\varphi$ are introduced and correspond with the associated variables. The definition of the divergence and gradient then become

$$\boldsymbol{\nabla h} = \frac{\partial h}{\partial \mathrm{r}}\mathbf{e}_\mathrm{r} + \frac{1}{\mathrm{r}}\frac{\partial h}{\partial \theta}\mathbf{e}_\theta + \frac{1}{\mathrm{r}\sin\theta}\frac{\partial h}{\partial \phi}\mathbf{e}_\varphi \tag{5}$$

$$\nabla \cdot \mathbf{q} = \frac{1}{\mathrm{r}^2}\frac{\partial\left(\mathrm{r}^2 \mathrm{q}_\mathrm{r}\right)}{\partial \mathrm{r}} + \frac{1}{\mathrm{r}\sin\theta}\frac{\partial\left(\sin\theta \mathrm{q}_\theta\right)}{\partial\theta} + \frac{1}{\mathrm{r}\sin\theta}\frac{\partial \mathrm{q}_\varphi}{\partial\varphi} \tag{6}$$

where $\mathbf{q} = \left[\mathrm{q}_\mathrm{r}, \mathrm{q}_\theta, \mathrm{q}_\varphi\right]$ is the specific discharge vector. Note that the specific discharge in radial direction, q_r, and recharge, q_r, are two different variables, so their corresponding symbols must not be confused. We are using spherical shell coordinates and it follows that $\mathrm{r} = R$, which is the mean radius of Mars, a constant. Equations (5) and (6) are reduced as follows

$$\nabla \boldsymbol{h} = \frac{1}{R}\frac{\partial h}{\partial\theta}\mathbf{e}_\theta + \frac{1}{R\sin\theta}\frac{\partial h}{\partial\varphi}\mathbf{e}_\varphi \tag{7}$$

$$\nabla \cdot \mathbf{q} = \frac{1}{R\sin\theta}\frac{\partial\left(\sin\theta \mathrm{q}_\theta\right)}{\partial\theta} + \frac{1}{R\sin\theta}\frac{\partial \mathrm{q}_\varphi}{\partial\varphi} \tag{8}$$

The discrete divergence and gradient operators in Cartesian coordinates are augmented to formulate the discrete operators in spherical shell coordinates for a logically rectangular grid using the curvilinear coordinate transformation. The rectangular domain is discretized into N_θ cells in θ direction and N_φ cells in φ direction. Therefore, the total number of cells are $N = N_\theta \times N_\varphi$. Moreover, the number of faces with normal in θ direction are $N_{f\theta} = (N_\theta + 1)N_\varphi$. Similarly the number of faces with normal in φ direction are $N_{f\varphi} = N_\theta(N_\varphi + 1)$. Therefore, the total number of faces, N_f, are $N_{f\theta} + N_{f\varphi} = (N_\theta + 1)N_\varphi + N_\theta(N_\varphi + 1)$.

For 1-D problem in polar θ coordinates which is discretized into N_θ cells, the discrete divergence operator, $\mathbf{D}_\theta^1$, takes the form

$$\mathbf{D}_\theta^1 = \frac{1}{R\Delta\theta} \underbrace{\begin{bmatrix} \frac{1}{\sin\theta_{c_1}} & & \\ & \ddots & \\ & & \frac{1}{\sin\theta_{c_{N_\theta}}} \end{bmatrix}}_{N_\theta \ \times \ N_\theta} \underbrace{\begin{bmatrix} -1 & 1 & & \\ & \ddots & \ddots & \\ & & -1 & 1 \end{bmatrix}}_{N_\theta \ \times \ N_{\theta+1}} \underbrace{\begin{bmatrix} \sin\theta_{f_1} & & \\ & \ddots & \\ & & \sin\theta_{f_{N_\theta+1}} \end{bmatrix}}_{N_{\theta+1} \ \times \ N_{\theta+1}} \tag{9}$$

where $\sin\theta_c$ is the co-latitude at the cell center and $\sin\theta_f$ is the co-latitude at the cell face. The Kronecker product gives the 2-D polar direction discrete divergence, $\mathbf{D}_\theta$

$$\mathbf{D}_\theta = \mathbf{D}_\theta^1 \otimes \mathbf{I}_\varphi, \tag{10}$$

where $\mathbf{I}_\varphi$ is $N_\varphi \times N_\varphi$ identity matrix.

Similarly, the 1-D discrete gradient for the polar coordinates, $\mathbf{G}_\theta^1$, can be derived as

$$\mathbf{G}_\theta^1 = \frac{1}{R\Delta\theta} \underbrace{\begin{bmatrix} 0 & & & & \\ -1 & 1 & & & \\ & \ddots & \ddots & & \\ & & & -1 & 1 \\ & & & & 0 \end{bmatrix}}_{N_{\theta+1} \ \times N_\theta} \tag{11}$$

The Kronecker product gives the 2-D polar direction discrete gradient, $\mathbf{G}_\theta$ as

$$\mathbf{G}_\theta = \mathbf{G}_\theta^1 \otimes \mathbf{I}_\varphi. \tag{12}$$

The discrete gradient and divergence operators in azimuthal φ direction differ by the term '$\frac{1}{\sin\theta_c}$' from their corresponding polar counterparts, but are constructed in a similar fashion from 1-D operators. First, we generate the corresponding 1-D matrices with respect to φ. The 1-D divergence operator in azimuthal direction, $\mathbf{D}_\varphi^1$, takes the form

$$\mathbf{D}_\varphi^1 = \frac{1}{R\Delta\varphi} \underbrace{\begin{bmatrix} -1 & 1 & & \\ & \ddots & \ddots & \\ & & -1 & 1 \end{bmatrix}}_{N_\varphi \ \times \ N_{\varphi+1}} \tag{13}$$

Again, using the diagonal matrix of co-latitude of the cell center θ_c, $\mathbf{Sin}_{\theta_c,inv}$. The value of $\sin\theta_c$ varies with co-latitude, therefore the Kronecker product uses

$$\mathbf{Sin}_{\theta_c,inv} = \underbrace{\begin{bmatrix} \frac{1}{\sin\theta_{c_1}} & & \\ & \ddots & \\ & & \frac{1}{\sin\theta_{c_{N_\theta}}} \end{bmatrix}}_{N_\theta \ \times \ N_\theta} \tag{14}$$

to assemble the two-dimensional divergence in φ direction, $\mathbf{D}_\varphi$, as

$$\mathbf{D}_\varphi = \mathbf{Sin}_{\theta_c,inv} \otimes \mathbf{D}_\varphi^1. \tag{15}$$

The 1-D discrete gradient in the φ direction, $\mathbf{G}^1_\varphi$, becomes

$$\mathbf{G}^1_\varphi = \frac{1}{R\Delta\varphi} \underbrace{\begin{bmatrix} 0 & & & & \\ -1 & 1 & & & \\ & \ddots & \ddots & & \\ & & & -1 & 1 \\ & & & & 0 \end{bmatrix}}_{N_{\varphi+1} \times N_\varphi} \tag{16}$$

and the Kronecker product uses $\mathbf{Sin}_{\theta_c,inv}$ to form the 2-D discrete gradient in φ direction, $\mathbf{G}_\varphi$, as

$$\mathbf{G}_\varphi = \mathbf{Sin}_{\theta_c,inv} \otimes \mathbf{G}^1_\varphi. \tag{17}$$

The two-dimensional operators in θ and ϕ are finally assembled as

$$\mathbf{D} = \begin{bmatrix}\mathbf{D}_\theta \ \mathbf{D}_\varphi\end{bmatrix} \quad \text{and} \quad \mathbf{G} = \begin{bmatrix}\mathbf{G}_\theta \\ \mathbf{G}_\varphi\end{bmatrix}. \tag{18}$$

To enforce the periodic boundary conditions while using our discrete operators, we modify the operators appropriately. The divergence operator does not need modified [10]. However, the discrete 1-D gradient in azimuthal direction, $\mathbf{G}^1_\varphi$, needs to be changed to

$$\mathbf{G}^1_\varphi = \frac{1}{R\Delta\varphi} \underbrace{\begin{bmatrix} 1 & & & & -1 \\ -1 & 1 & & & \\ & \ddots & \ddots & & \\ & & & -1 & 1 \\ 1 & & & & -1 \end{bmatrix}}_{N_{\varphi+1} \times N_\varphi}. \tag{19}$$

Mean operator: Similar to the discrete gradient, the mean operator maps the cell centered values to cell faces [11]. The one-dimensional algebraic mean operator can be constructed in polar (θ) and azimuthal (φ) directions as follows

$$\mathbf{M}^1_\theta = \frac{1}{2}\begin{bmatrix} 2 & & & & & \\ 1 & 1 & & & & \\ & 1 & 1 & & & \\ & & \ddots & \ddots & & \\ & & & 1 & 1 & \\ & & & & 1 & 1 \\ & & & & & 2 \end{bmatrix}_{N_{\theta+1} \times N_\theta} \quad \text{and} \quad \mathbf{M}^1_\varphi = \frac{1}{2}\begin{bmatrix} 2 & & & & & \\ 1 & 1 & & & & \\ & 1 & 1 & & & \\ & & \ddots & \ddots & & \\ & & & 1 & 1 & \\ & & & & 1 & 1 \\ & & & & & 2 \end{bmatrix}_{N_{\varphi+1} \times N_\varphi}. \tag{20}$$

Here the cell center values at the boundary faces are moved to the faces without interpolating since they will be replaced by the boundary conditions.

The Kronecker product gives the two-dimensional mean operators in polar and azimuthal directions respectively as

$$\mathbf{M}_\theta = \mathbf{M}_\theta^1 \otimes \mathbf{I}_\varphi \quad \text{and} \quad \mathbf{M}_\varphi = \mathbf{I}_\theta \otimes \mathbf{M}_\varphi^1. \tag{21}$$

Finally, the two-dimensional N by N_f mean operator matrix, $\mathbf{M}$ can be constructed as

$$\mathbf{M} = \begin{bmatrix} \mathbf{M}_\theta \\ \mathbf{M}_\varphi \end{bmatrix}. \tag{22}$$

S2.3 Discretization of the governing equation

The governing Equation (1) takes the form

$$\phi_0\, \mathbf{h}_{i+1}^m \left(\mathbf{h}_{i+1} - \mathbf{h}_i\right) - \Delta t\, K_0\, \mathbf{D} \left[\left\{ \mathbf{M} \left(\frac{\mathbf{h}_{i+1}^{n+1}}{n+1} \right) \right\}_f \mathbf{G}\mathbf{h}_{i+1} \right] = \Delta t\, \mathbf{f}_{s,i}. \tag{23}$$

where the subscript i is the time step. Here the multiplication refers to the matrix-matrix or matrix-vector multiplications. The $N \times 1$ vectors $\mathbf{h}_{i+1}$ and $\mathbf{f}_{s,i}$ refer to the unknown solution and the source term, $\mathbf{f}_s$, at the cell centers of the discretized domain, respectively. Here $\{\mathbf{v}\}_f$ is an $N_f \times N_f$ diagonal matrix with $N_f \times 1$ vector $\mathbf{v}$ on the diagonal. This nonlinear governing equation (23) is solved at each time step i using the Newton-Raphson solver in as was done previously for a steady case in [12].

S2.4 Implementation of boundary conditions

The boundary conditions are implemented to make the system well-posed. The boundary conditions corresponding to the shorelines and craters move when they invade or retreat based on their filling or emptying, respectively. It is implemented using a constant head (heterogeneous Dirichlet boundary conditions) level set in a variable region. Homogeneous Dirichlet boundary condition (zero head) is implemented using constraint elimination. This elimination occurs through projection approach in which the full space of unknowns $\mathbb{R}^N$ is reduced to the space of reduced unknowns $\mathbb{R}^{(N-N_c)}$ when N_c number of constraints or Dirichlet boundary conditions are supplied. For heterogeneous Dirichlet boundary conditions, the (quasi-)linearity of the problem in the Newton iteration allows splitting of the solution into homogeneous and particular solutions followed by constraint elimination.

As discussed earlier in section S2.2, the homogeneous Neumann boundary (no-flux) are in-built in the discrete gradient operator by zeroing out the boundary terms. The heterogeneous Neumann boundary conditions are implemented simply by converting the flux entering or exiting the cell through cell faces into a source term corresponding to those cells.

$$q_{r,n} = \mathrm{q}_n * \frac{A_n}{V_n} \tag{24}$$

where $q_{r,n}$ is the recharge/source term at the cells with volume V, corresponding to Neumann boundary. The flux q_n is the input Neumann boundary condition at the face with area A_n. The resulting source term from Neumann boundary, $q_{r,n}$, is added to the source term of the discrete governing equation corresponding to cells with Neumann boundary condition. See the appendix of [11] for a more detailed description of the boundary condition implementation.

S2.5 Treatment of irregular domains

Since shoreline as well as crater boundaries are not straight and can move, the domain needs to be cropped out irregularly of the solution. This is done to keep the system well-posed. In this logically regular tensor grid framework, it is relatively easy to find the degrees of freedom of the inactive cells corresponding to the crater or northern ocean (see Figure S1a). Once the inactive cells are found, the active cells are located where the discrete governing equation needs to be solved. Moreover, the boundary face between the active and inactive regions can be located using the information from the divergence operator, $\mathbf{D}$, which connects cell faces to cell centers (see Figure S1b). Both active and inactive cells lying immediately next to boundary condition are crucial, since the boundary condition is now applied to those cells. The entries corresponding to inactive cells can be removed from the matrix equation using projection approach once Dirichlet boundary condition is specified, as discussed briefly in section S2.4. In this process, the boundary is set to natural, similar to typical boundary conditions by zeroing out the rows corresponding to the divergence entries of active cells lying on the domain boundary. The reduced matrix system of discrete governing equations can then be solved on the active cells (see Figure S1c).

S3 Derivation of $\bar{r}/\bar{K}$ and compatible groundwater dynamics

This section describes the calculations used to generate Tables S1–S3. These tables convert prescribed runoff intensities into regional groundwater recharge rates, then calculate the maximum intermittency and number of runoff episodes that remain compatible with the groundwater threshold from the transient aquifer simulations.

Here q_{run} is the surface runoff intensity (specific flux, mm day^{-1}) reported or assumed from geomorphic or climate constraints. The quantity f_r is the infiltration or recharge fraction, defined as the fraction of total precipitation that becomes regional groundwater recharge. The quantity r_{rech} is the recharge intensity during runoff-producing intervals, $\bar{r}$ is the time-averaged recharge rate, I is the intermittency or duty cycle, $\bar{K}$ is the vertically averaged hydraulic conductivity of the aquifer, and

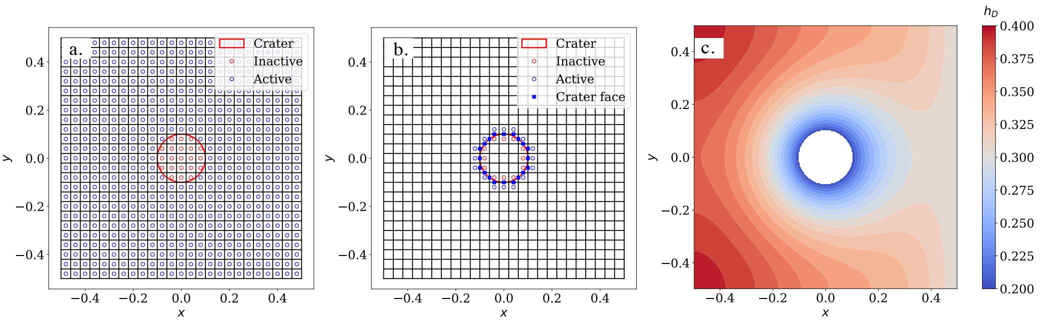

Fig. S1 An example of solving a problem on a domain with an addition irregular boundary (a circular crater). (a) Find the inactive and active cells. (b) Find the boundary of the irregular domain and moreover, inactive and active cells adjacent to that boundary using information from the divergence operator, **D**. (c) Solve the reduced system on active cells by setting the boundary conditions on active cells shown in (b). This figure shows the dimensionless head solution contours by solving a Poisson equation, $\nabla \cdot \nabla h_D = 1$, in Cartesian coordinates. The unit square domain [-0.5,0.5]×[-0.5,0.5] is divided uniformly into 25×25 cells. The domain boundary ($x = -0.5, x = 0.5, y = -0.5, y = 0.5$) is set to $h_D = 0.3$ whereas the crater boundary is set to $h_D = 0.2$.

$(\bar{r}/\bar{K})_{\text{crit}}$ is the groundwater-compatible recharge to conductivity threshold. The individual runoff episode duration is denoted by τ, and the total valley network forming interval considered here is T_{form}.

Runoff to recharge conversion

We neglect evaporation in this comparison. Total precipitation is therefore partitioned only into surface runoff and regional groundwater recharge,

$$P = q_{\text{run}} + r_{\text{rech}}. \tag{25}$$

The recharge fraction is defined as

$$f_r = \frac{r_{\text{rech}}}{P}. \tag{26}$$

Similarly, the runoff fraction is

$$1 - f_r = \frac{q_{\text{run}}}{P}. \tag{27}$$

Solving equations 26 and 27 for recharge in terms of runoff gives

$$r_{\text{rech}} = q_{\text{run}} \frac{f_r}{1 - f_r}. \tag{28}$$

Thus, when runoff is reported in mm day^{-1}, the recharge rate during wet intervals is converted to years as:

$$r_{\text{rech}} = q_{\text{run}} \times 365.25 \times \frac{f_r}{1 - f_r}, \tag{29}$$

where q_{run} is in mm day^{-1} and r_{rech} is in mm yr^{-1}.

Groundwater compatible intermittency

The transient groundwater simulations are organized by the time averaged recharge to conductivity ratio,

$$\left(\frac{r}{K}\right)_{\text{ta}} = \frac{\bar{r}}{\bar{K}}. \tag{30}$$

For intermittent recharge,

$$\bar{r} = I r_{\text{rech}}, \tag{31}$$

where

$$I = \frac{t_{\text{on}}}{t_{\text{on}} + t_{\text{off}}}. \tag{32}$$

Substituting equation 28 into equation 30 gives the nominal runoff derived recharge to conductivity ratio,

$$\left(\frac{r}{K}\right)_{\text{ta}} = \frac{q_{\text{run}}\left(\frac{f_r}{1-f_r}\right) I}{\bar{K}} = \frac{\bar{r}}{\bar{K}}. \tag{33}$$

No geometric recharge weighting coefficient, C_r, is applied in this literature comparison due to uncertainties in the global distribution of the run off and the first order nature of the weighting coefficient. The values in Tables S1–S3 are therefore nominal time-averaged $\bar{r}/\bar{K}$ values and event count limits, not model geometry weighted recharge values.

We use

$$\bar{K} = 3.3678 \text{ m yr}^{-1} = 3367.8 \text{ mm yr}^{-1}, \tag{34}$$

and the groundwater-compatible threshold

$$\left(\frac{\bar{r}}{\bar{K}}\right)_{\text{crit}} = 10^{-5}. \tag{35}$$

The corresponding critical time averaged recharge rate is

$$\bar{r}_{\text{crit}} = \bar{K}\left(\frac{\bar{r}}{\bar{K}}\right)_{\text{crit}}. \tag{36}$$

Using equations 34 and 35,

$$\bar{r}_{\text{crit}} = 3367.8 \times 10^{-5} = 3.37 \times 10^{-2} \text{ mm yr}^{-1}. \tag{37}$$

For a prescribed runoff intensity and recharge fraction, the maximum groundwater-compatible intermittency is obtained by setting $\bar{r} = \bar{r}_{\text{crit}}$,

$$I_{\max} = \frac{\bar{r}_{\text{crit}}}{r_{\text{rech}}}. \tag{38}$$

Substituting equation 29 gives

$$I_{\max} = \frac{0.033678}{q_{\text{run}} \times 365.25 \times \left(\frac{f_r}{1-f_r}\right)}, \tag{39}$$

where q_{run} is in mm day^{-1}. This is the equation used to calculate $I_{\max}$ in Tables S1–S3.

Fluvial working time and event counts

The cumulative wet or fluvial working time allowed within a total formation interval T_{form} is

$$T_{\mathrm{wet}} = I_{\max} T_{\mathrm{form}}. \tag{40}$$

For the calculations in Tables S1–S3, we use

$$T_{\mathrm{form}} = 100 \text{ Myr} = 10^8 \text{ yr}. \tag{41}$$

Thus,

$$T_{\mathrm{wet}} = I_{\max} \times 10^8 \text{ yr}. \tag{42}$$

The number of runoff-producing episodes of duration τ that can occur within this wet-time budget is

$$N_\tau = \frac{T_{\mathrm{wet}}}{\tau}. \tag{43}$$

Combining equations 42 and 43 gives

$$N_\tau = \frac{I_{\max} \times 10^8}{\tau}, \tag{44}$$

where τ is in years. Tables S1–S3 report N_τ for $\tau = 10^2$, 10^3, 10^4, and 10^5 yr, corresponding to the episode-duration range motivated by Stucky de Quay et al.-style runoff episodes.

Values of $N_\tau < 1$ indicate that even one runoff episode of duration τ would exceed the groundwater-compatible wet-time budget for the specified runoff rate and recharge fraction.

Equivalent cycle period and dry interval

The maximum intermittency can also be expressed in terms of an event recurrence structure. For an individual runoff episode of duration τ, the full wet-dry cycle period is

$$T_{\mathrm{cycle}} = \frac{\tau}{I_{\max}}. \tag{45}$$

The dry interval between runoff episodes is

$$t_{\mathrm{dry}} = T_{\mathrm{cycle}} - \tau, \tag{46}$$

or equivalently,

$$t_{\mathrm{dry}} = \tau \left(\frac{1 - I_{\max}}{I_{\max}} \right). \tag{47}$$

Tables S1–S3 report the same constraint in terms of event counts rather than cycle periods. The two descriptions are equivalent because

$$N_\tau = \frac{T_{\rm form}}{T_{\rm cycle}} = \frac{I_{\max} T_{\rm form}}{\tau}. \tag{48}$$

Table S1 Groundwater-compatible event counts for daily runoff intensities of 1–10 mm day^{-1}, using infiltration fractions of 0.1%, 1%, and 22%, without applying C_r.

$q_{\rm run}$ (mm day^{-1})	Infiltration fraction	$r_{\rm rech}$ (mm yr^{-1})	$I_{\max}$	Fluvial working time in 100 Myr	$N_{100\,\rm yr}$	$N_{1\,\rm kyr}$	$N_{10\,\rm kyr}$	$N_{100\,\rm kyr}$
1	0.1%	0.366	9.21%	9.21 Myr	92,113	9,211	921	92.1
1	1%	3.69	0.913%	0.913 Myr	9,128	913	91.3	9.13
1	22%	103.02	0.0327%	0.0327 Myr	327	32.7	3.27	0.327
5	0.1%	1.83	1.84%	1.84 Myr	18,423	1,842	184	18.4
5	1%	18.45	0.183%	0.183 Myr	1,826	183	18.3	1.83
5	22%	515.10	0.00654%	0.00654 Myr	65.4	6.54	0.654	0.0654
10	0.1%	3.66	0.921%	0.921 Myr	9,211	921	92.1	9.21
10	1%	36.89	0.0913%	0.0913 Myr	913	91.3	9.13	0.913
10	22%	1030.19	0.00327%	0.00327 Myr	32.7	3.27	0.327	0.0327

Notes: $q_{\rm run}$ is the runoff intensity. The infiltration fraction is the fraction of total precipitation that becomes regional groundwater recharge. In the calculation, f_r is used as a dimensionless fraction, so 0.1%, 1%, and 22% correspond to $f_r = 0.001$, 0.01, and 0.22, respectively. Evaporation is neglected, so $r_{\rm rech} = q_{\rm run} \times 365.25 \times f_r/(1 - f_r)$. The groundwater-compatible duty cycle is $I_{\max} = \bar{r}_{\rm crit}/r_{\rm rech}$, where $\bar{r}_{\rm crit} = \bar{K}\,(\bar{r}/\bar{K})_{\rm crit} = 0.033678$ mm yr^{-1}. Event counts are calculated as $N_\tau = I_{\max} T_{\rm form}/\tau$, with $T_{\rm form} = 100$ Myr. No geometric recharge coefficient, C_r, is applied. Values of $N_\tau < 1$ indicate that even one event of that duration would exceed the groundwater-compatible wet-time budget.

Table S2 Groundwater-compatible event counts for 100 mm day^{-1} runoff, without applying C_r.

$q_{\rm run}$ (mm day^{-1})	Infiltration (%)	$r_{\rm rech}$ (mm yr^{-1})	$I_{\max}$	Wet time in 100 Myr	$N_{100\,\rm yr}$	$N_{1\,\rm kyr}$	$N_{10\,\rm kyr}$	$N_{100\,\rm kyr}$
100	1%	368.94	0.00913%	9.13 kyr	91.3	9.13	0.913	0.0913
100	0.1%	36.56	0.0921%	92.1 kyr	921	92.1	9.21	0.921

Notes: Infiltration is reported as the percentage of total precipitation that becomes regional groundwater recharge. In the calculation, 1% and 0.1% correspond to $f_r = 0.01$ and $f_r = 0.001$, respectively. Evaporation is neglected, so $r_{\rm rech} = q_{\rm run} \times 365.25 \times f_r/(1 - f_r)$. The groundwater-compatible duty cycle is $I_{\max} = \bar{r}_{\rm crit}/r_{\rm rech}$, where $\bar{r}_{\rm crit} = \bar{K}\,(\bar{r}/\bar{K})_{\rm crit} = 0.033678$ mm yr^{-1}. Event counts are calculated as $N_\tau = I_{\max} T_{\rm form}/\tau$, with $T_{\rm form} = 100$ Myr. No geometric recharge coefficient, C_r, is applied. Values of $N_\tau < 1$ indicate that even one event of that duration would exceed the groundwater-compatible wet-time budget.

Table S3 Groundwater-compatible event counts for 100 mm day^{-1} runoff using infiltration percentages of .01% and .001%, without applying C_r.

q_{run} (mm day^{-1})	Infiltration (%)	r_{rech} (mm yr^{-1})	$I_{\max}$	Wet time in 100 Myr	$N_{100\,\mathrm{yr}}$	$N_{1\,\mathrm{kyr}}$	$N_{10\,\mathrm{kyr}}$	$N_{100\,\mathrm{kyr}}$
100	.01%	3.65	0.922%	0.922 Myr	9,220	922	92.2	9.22
100	.001%	0.365	9.22%	9.22 Myr	92,200	9,220	922	92.2

Notes: Infiltration is reported as a percentage of total precipitation that becomes regional groundwater recharge. In the calculation, .01% and .001% correspond to $f_r = 10^{-4}$ and $f_r = 10^{-5}$, respectively. Evaporation is neglected, so $r_{\mathrm{rech}} = q_{\mathrm{run}} \times 365.25 \times f_r/(1 - f_r)$. The groundwater-compatible duty cycle is $I_{\max} = \bar{r}_{\mathrm{crit}}/r_{\mathrm{rech}}$, where $\bar{r}_{\mathrm{crit}} = \bar{K}\,(\bar{r}/\bar{K})_{\mathrm{crit}} = 0.033678$ mm yr^{-1}. Event counts are calculated as $N_\tau = I_{\max}T_{\mathrm{form}}/\tau$, with $T_{\mathrm{form}} = 100$ Myr. No geometric recharge coefficient, C_r, is applied. Values of $N_\tau < 1$ indicate that even one event of that duration would exceed the groundwater-compatible wet-time budget.

Supplementary Video 1

Animation of representative transient groundwater simulations through successive recharge and intra-recharge intervals (5 kyr recharge periods separated by 1 Myr intra-recharge intervals). The animation shows the evolving groundwater table elevation, z_{GW}; the groundwater margin $\Delta z = z_{\mathrm{GW}} - z_{\mathrm{VN}}$ relative to the valley networks; and the resulting valley network density weighted flooded fraction, F_{VN}, as a function of time, for the three representative recharge rates $r = 30$, 90, and 190 mm yr^{-1}, corresponding to $\bar{r}/\bar{K} = 1.5\times10^{-5}$, 4.4×10^{-5}, and 9.3×10^{-5}. The animation is a dynamic companion to Figs. 2 and 3 of the main text.

References

[1] Dupuit, J.: Etudes Théoriques et Pratiques sur Le Mouvement des Eaux dans les Canaux Découverts et Àtravers les Terrains perméable, 2nd edn., pp. 1–304. Dunod, Paris (1863)

[2] Forchheimer, P.: Wasserbewegung durch Boden. Zeitschrift des Vereins Deutscher Ingenieure **45**, 1782–1788 (1901)

[3] Boussinesq, J.V.: Théorie Analytique de la Chaleur. Gauthier-Villars, Paris (1903)

[4] Batchelor, G.K.: An Introduction to Fluid Dynamics, p. 658. Cambridge University Press, Cambridge (2000)

[5] Shadab, M.A., Hiatt, E., Bahia, R.S., Bohacek, E.V., Steinmann, V., Hesse, M.A.: Infiltration dynamics on early mars: Geomorphic, climatic, and water storage implications. Geophysical Research Letters **52**(8), 2024–111939 (2025)

[6] Shadab, M.A., Hiatt, E., Hesse, M.: Investigating groundwater dynamics and residence times on early mars using unconfined aquifer model with vertical

heterogeneity. LPI Contributions, 1736 (2023)

[7] LeVeque, R.J.: Numerical Methods for Conservation Laws, 2nd edn. Birkhäuser Verlag, Basel (1992)

[8] Veiga, L.B., Lipnikov, K., Manzini, G.: The Mimetic Finite Difference Method for Elliptic Problems. Springer, Cham (2014). https://doi.org/10.1007/978-3-319-02663-3 . http://link.springer.com/10.1007/978-3-319-02663-3

[9] Haber, E.: Computational Methods in Geophysical Electromagnetics, 1st edn., pp. 1–144. Society for Industrial and Applied Mathematics, Vancouver (2015)

[10] Hesse, M.A., Castillo-Rogez, J.C.: Thermal Evolution of the Impact-Induced Cryomagma Chamber Beneath Occator Crater on Ceres. Geophysical Research Letters **46**(3), 1121–1888 (2019) https://doi.org/10.1029/2018GL080327

[11] Shadab, M.A., Hesse, M.A.: A hyperbolic–elliptic pde model and conservative numerical method for gravity-dominated variably-saturated groundwater flow. Advances in Water Resources **190**, 104736 (2024)

[12] Hiatt, E., Shadab, M.A., Gulick, S.P., Goudge, T.A., Hesse, M.A.: Limited recharge of the southern highlands aquifer on early mars. Icarus **408**, 115774 (2024)